Charge Recognition in Ru(bpy)₃²⁺ on a Metal Surface via Ultrahigh Vacuum Tip-Enhanced Raman Spectroscopy

Sayantan Mahapatra,¹ Chamath Siribaddana,¹ Linfei Li,¹ Soumyajit Rajak,¹ Xu Zhang,² and Nan Jiang^{1,3} *

¹Department of Chemistry, University of Illinois Chicago, Chicago, Illinois 60607, United States

²Department of Physics and Astronomy, California State University, Northridge, California 91330, United States

³Department of Physics, University of Illinois Chicago, Chicago, Illinois 60607, United States

Abstract

Ruthenium-based dye molecules hold great promise in the photochemistry and electrochemistry research fields, ranging from photocatalysis and luminescence to thermal imaging and photodynamic therapy. However, despite this exciting prospect, thermal sublimation and surface characterization of these molecules under the ultrahigh vacuum (UHV) is rare. Here, we achieved successful thermal sublimation of Tris(2,2'-bipyridine)-ruthenium(II) [Ru(bpy)3²⁺] onto the Cu(100) surface and investigated the surface decoration using scanning tunneling microscopy (STM) and non-resonance tip-enhanced Raman spectroscopy (STM-TERS). The experimental findings are complemented by density functional theory (DFT) and time-dependent DFT (TDDFT) calculations. Integrating experimental and theoretical analyses facilitates the chemical characterization of Ru(bpy)3²⁺ molecules at the single-molecule level, encompassing their charged state and surface aggregation. Our analysis indicates no quenching of charge or significant charge transfer from the Cu surface to the molecule's core. The results here provide important chemical

insight into ruthenium-based dye molecules essential for photochemistry and electrochemistryrelated applications.

1. Introduction

Investigating the response and influence of metallic surfaces toward external electric field sources is of paramount interest for electrode-electrolyte interfaces, 1 spin dynamics, 2 and so forth which affect applications ranging from renewable energy production to materials processing.³ For instance, when a multiply charged system (such as ions or molecules) approaches a metal surface, it can be viewed as a collection of potential energy, with the main concern being the charge neutralization on the metal surface.³ It depends on how the charged molecule interacts with the underlying substrate. Therefore, charge recognition and local chemistry (single-molecule level information) in surface-adsorbed systems are extremely essential for understanding complex activity, reactivity, charge distribution, and self-assembly processes. Scanning tunneling microscopy (STM) offers a direct route to image and visualize the surface-adsorbed molecules (topographic information) with an atomic spatial resolution by detecting tunneling current between the tip and sample.⁴⁻⁵ However, directly adsorbed molecules on a metallic surface are rarely differentiated between their charged and neutral states by STM.⁶⁻⁷ Therefore, examining the chemical characteristics of surface-bound molecules at the single-molecule level is essential because even slight alterations in geometry or symmetry reduction can cause variations in the vibrational features of the charged and neutral states.

Tip-enhanced Raman spectroscopy (TERS), a tandem technique of STM with optical spectroscopy, offers a way to receive topographic images of single molecules and chemical identification through Raman spectroscopy, simultaneously.⁸⁻¹⁸ By confining light at a plasmonically active metallic tip apex (made of Ag or Au) and taking advantage of plasmon-

enhanced Raman scattering,¹⁹ TERS can investigate nanoscale chemistry ranging from biomolecules,²⁰⁻²⁵ two-dimensional materials,²⁶⁻³⁰ catalytic systems,³¹⁻³⁶ to molecular self-assembly³⁷⁻⁴⁴ and so forth. Recent high-resolution TERS studies also allow chemical bonds to be resolved and mapped inside a single molecule.⁴⁵⁻⁵⁰ However, there are no reports of TERS being used to directly detect charge states within a molecule on a metal surface.

Herein, we report a combined STM and TERS investigation to probe a charged rutheniumbased dye molecule on an atomically flat Cu(100) surface, managing to recognize the charged state of the molecule. Ruthenium-based dye molecules have aroused significant interest in the photochemistry⁵¹⁻⁵² and electrochemistry⁵³⁻⁵⁴ research fields, ranging from photocatalysis,⁵⁵ and electrochemiluminescence⁵⁶ to dye-sensitized solar cells for solar energy.⁵⁷ Moreover, these dyes are significantly useful in applications such as two-photon three-dimensional thermal imaging⁵⁸ and molecular encoder-decoder.⁵⁹ Despite this exciting prospect, however, surface visualization and characterization of these types of dye molecules are rare.⁶⁰ The prototypical molecule, Tris(2,2'-bipyridine)-ruthenium(II) (referred to as Ru(bpy)₃²⁺, Figure 1) consists of a central ruthenium core (in +2 oxidation state) with three bipyridine (bpy) functional groups in the octahedrally coordinated geometry (D₃ symmetry). The primary electronic absorption in the UVvisible spectrum at around 452 nm is controlled by the central Ru(II) core through a metal-toligand charge transfer (MLCT) transition.⁶¹ This particular molecule is chosen due to the fact that bipyridine ligands are expected to lift the molecule away from the surface, thereby aligning better with the plasmonic dipole at the tip-sample nano-junction. In this study, the STM-combined TERS approach was utilized to observe and chemically distinguish individual Ru(bpy)₃²⁺ molecules on a Cu(100) surface. Furthermore, considering the charge neutralization process, density functional theory (DFT) and time-dependent DFT (TDDFT) simulations reveal slight differences in the

vibrational spectra of the charged and neutral states [i.e., Ru(bpy)₃²⁺ and Ru(bpy)₃] on Cu(100). Through a comparison between theoretical and experimental outcomes, we can determine the charged state of the molecule at the single-molecule level. In addition to elucidating the molecular surface morphology, adsorption configuration, and charged state on Cu(100), this work demonstrates the surface aggregation of these molecules which sheds light on generating charged nano-arrays in the future. While few studies have explored the surface-enhanced Raman spectroscopy (SERS) of Ru(bpy)₃²⁺, this marks the first report of TERS for Ru(bpy)₃²⁺, to the best of our knowledge.

2. Experimental and Theoretical Methods

The experiments were conducted within a variable temperature STM system (UNISOKU, USM1400) maintained under a base pressure of 4 ×10⁻¹¹ torr. The clean surface of Cu(100) single crystal sample was prepared in a preparation chamber (base pressure 1 × 10⁻¹⁰ torr), isolated from the STM chamber by a gate valve. The Cu(100) surface underwent thorough cleaning through repetitive cycles of Argon ion sputtering (1 kV, ~2.5 × 10⁻⁵ torr) and subsequent indirect thermal annealing up to 865 K. The Ru(bpy)3²⁺ molecules [Tris(2,2'-bipyridine)dichloro-ruthenium(II) hexahydrate, C30H24Cl2N6Ru · 6H2O] were purchased from Sigma Aldrich (purity > 99%). The powder was degassed prior to deposition at 410 K for several hours, which got rid of the crystalline H2O molecules. Following that, they were sublimed onto the Cu(100) surface via a K-cell molecular evaporator (ACME Technology Co., Ltd.) for 1 min (190 °C) for sub-monolayer coverage. During thermal sublimation inside UHV, the molecules are anticipated to be deposited as di-cationic species onto the metal surface.⁶² The sample remained at room temperature during the deposition process. Subsequently, it was transferred to the STM chamber for both STM imaging and Raman spectroscopy experiments, conducted at a low temperature of liquid nitrogen

(78 K). Electrochemically etched Ag tips were employed for both STM imaging and TERS experiments.⁶³ To ensure optimal performance, the plasmonically active Ag tips underwent a cleaning process in the preparation chamber involving Argon ion sputtering (1.5 kV, \sim 2.5 × 10⁻⁵ Torr) before their utilization in STM and TERS experiments.

TERS experiments employed a 633 nm continuous wave (cw) HeNe laser (LASOS) with polarization parallel to the tip, functioning as the incoming photon source. Detection of the TERS signal utilized an iso-plane SCT320 spectrograph (Princeton Instrument) in combination with a Princeton Instrument PIXIS 100 CCD. A detailed illustration of the home-built optical setup has been provided in previous literatures.⁶³⁻⁶⁴

DFT simulations were performed to calculate the adsorption of charged- and neutral-Ru(bpy)₃ molecules on the Cu(100) surface, which is modeled by a four-layer slab with a (5 × 5) unit cell. The DFT calculations were carried out using the VASP package⁶⁵ with the projector augmented wave pseudopotentials⁶⁶ and the Perdew-Burke-Ernzerhof generalized gradient approximation.⁶⁷ An energy cutoff of 400 eV was used for the plane-wave basis set. Only the Γ-point in the Brillouin zone was used considering the large size of the supercell. The van der Waals (vdW) interaction was included by using a non-local correlation functional.⁶⁸ The nonlocal correlation functional is expressed in terms of a density-density interaction formula with a relatively simple parametrized kernel,⁶⁸ which is numerically determined in a plane-wave basis. The atoms in the bottom two layers of the Cu(100) slab were fixed in their equilibrium positions while the rest of the atoms were fully relaxed. The force convergence criterion is 0.01 eV/Å for the structural optimization. The phonon modes of the adsorbed Ru(bpy)₃ molecules were obtained in the presence of the Cu(100) surface (which was kept frozen) by solving the eigenvalue problems of a dynamical or Hessian matrix based on density functional perturbation theory calculations.⁶⁹

TDDFT calculations⁷⁰ were employed to determine the Raman intensity of the charged- and neutral-Ru(bpy)₃ molecules with the adsorption configuration.

3. Results and Discussion

3.1. Scanning Tunneling Microscopy

Rubpy is an ionic organometallic species [Ru(bpy)₃²⁺] and thus belongs to a class of molecules that are seldom used for UHV deposition. Electrospray ion beam deposition (ES-IBD) at suitable energies can successfully deposit ionic Rubpy molecules or molecular fragments onto surfaces under UHV conditions.⁷¹ In this present work, we successfully achieved the thermal sublimation of these ionic Rubpy molecules onto a Cu(100) surface at a pressure of $<1 \times 10^{-10}$ torr. Surface decoration was first demonstrated using constant-current STM topography measurements after the Ru(bpy)₃²⁺ molecules were deposited at room temperature. Figure 1a shows a large-scale STM image, where molecules appear as a "dumbbell-shaped" structure, consisting of two similar ellipsoidal-shaped bright protrusions. Considering the dimensions of a gas-phase Ru(bpv)₃²⁺ molecule (octahedrally coordinated geometry), we can assign each bright protrusion to one molecule, ultimately resulting in the formation of a molecular dimer (Supporting Information, Figure S1). A thorough examination indicates that these two molecules in the dimer arrangement are generally oriented parallel to each other (as marked by the green dotted ellipsoids in Figures 1b–d), and their separation distance varies from around ~ 0.70 nm to ~ 1.35 nm (as shown in Figures 1b-d, Supporting Information, Figure S2). Furthermore, the majority of the molecular dimers are observed with an intermolecular spacing of 1.01 ± 0.04 nm (Figures 1b-c). It is noteworthy that when the intermolecular spacing increases slightly (e.g., ~1.35 nm as shown in Figure 1d), the individual molecules seem to exhibit slight deviations from their parallel alignment. Additionally, molecular aggregations (e.g. dimer structures) were observed to align closely in one

of two orientations on the surface relative to the close-packed directions of the (100) substrate, each with equal probability (Figures 1a–d).

As STM severely lacks chemical sensitivity, it cannot provide conclusive information about the local chemistry of nonplanar surface adsorbates, such as adsorption configuration, and chemical interaction with a substrate. On the other hand, Raman spectroscopy continues to be an appealing technique for identifying the chemical signature of a molecule by examining its vibrational modes. Therefore, after revealing the topographic features, we supplement the STM-based results with single-molecule TERS measurements, enabling a complete nanoscale chemical identification of these molecules.

3.2. Non-Resonance Tip-Enhanced Raman Spectroscopy

Ru(bpy)₃²⁺ molecules were previously investigated through surface-enhanced Raman spectroscopy (SERS) and surface-enhanced hyper Raman spectroscopy (SEHRS).⁷² These techniques, however, are limited by ensemble averaging and, consequently, are influenced by multiple molecules within the laser spot size. To achieve a comprehensive understanding, nanoscale spectroscopic data on the same molecules imaged by STM can offer local chemical insights, establishing a direct link between topographical and chemical information for a specific surface area. In this context, STM-TERS emerges as a valuable tool for probing localized surface structure. By directing laser light at the tip–sample junction of STM, STM-TERS enables the detection of enhanced Raman fingerprints at the single-molecule level (Figure 2a). Recent studies have demonstrated the visualization of vibrational normal Raman modes for a single molecule absorbed on a Cu(100) surface using TERS.⁷³ Moreover, high-resolution TERS offers crucial insights into the newly synthesized two-dimensional (2D) material, borophene,⁷⁴ and its interactions with organic and small molecules with exceptional single-chemical-bond

sensitivity.⁷⁵⁻⁷⁷ Hence, we complement our findings derived from STM with TERS, ensuring a thorough chemical characterization of Ru(bpy)₃²⁺ molecules on the Cu(100) substrate.

When the incident photon energy closely matches the electronic transition [from the highest occupied molecular orbital (HOMO) to the lowest unoccupied molecular orbital (LUMO)] of the molecular system, the resonance Raman effect significantly enhances Raman scattering intensity. This phenomenon enables precise chemical analysis of surface-adsorbed molecular systems with single-molecule sensitivity. Recent reports have demonstrated angstrom-scale chemical characterization, such as identifying two porphodilactone isomers using resonant TERS in the visible region with a red laser (633 nm, 1.95 eV). However, for Ru(bpy)3²⁺ molecules with optical absorption (MLCT) mainly in the early visible region (452 nm, 2.74 eV), employing the same 633 nm laser for excitation results in non-resonant Raman scattering. Non-resonance Raman scattering is inherently weak, posing challenges in resolving molecular structures compared to the resonance Raman process. Our work, presented here, reports multiple enhanced Raman peaks from the adsorbed single Ru(bpy)3²⁺ molecule on the Cu(100) surface due to our unique design consisting piezo-driven *in-vacuo* excitation and collection lenses with large numerical apertures (NA = 0.4).

Figure 2b presents the single-molecule TERS measurements. It is worth noting that the Raman spectrum remains featureless when the distance between the tip and sample is relatively large under the scanning parameters of $I_t = 1$ nA and V = 1.0 V. However, upon approaching the tip and parking it over a single molecule (as indicated by the red circle in Figure 2a) with a higher current of $I_t = 4$ nA and a lower voltage of V = 0.1 V, multiple distinct Raman peaks of the adsorbed molecule are detected, as shown in Figure 2b (red spectrum). The amplified Raman signal can be explained by the decreased distance between the tip and the sample, resulting in improved

plasmonic field confinement at the tip apex for better detection of single molecules. In contrast, the Raman spectra obtained with the tip engaged on the Cu surface (green spectrum, $I_t = 4$ nA and V = 0.1 V) and with the tip retracted (black spectrum) are featureless, indicating that the Ag tip remains uncontaminated during the data acquisition and that the enhanced Raman signal arises from the molecule beneath the tip. Furthermore, the STM images before and after the TERS experiments (Supporting Information, Figure S3) confirm that the dimer structures remain intact and unaltered, validating the stability of the molecules under our experimental conditions.

In an effort to gain a complete understanding of the experimental TERS spectrum of the Ru(bpy)₃²⁺ molecule along with the corresponding binding configuration and the charged state, we performed DFT and TDDFT calculations. First, we performed DFT simulations to obtain the energetically favorable adsorption configurations of these molecules on the Cu(100) surface. Our simulation suggests two possible configurations for a charged-Ru(bpy)₃ molecule [i.e., Ru(bpy)₃²⁺] on Cu(100), that is, Configuration 1 (Figure 3a) and Configuration 2 (Supporting Information, Figure S4). According to the calculations, charged Configuration 1 is more energetically stable (by 0.49 eV) than charged Configuration 2. Additionally, we conducted DFT simulations for a neutral-Ru(bpy)₃ molecule [i.e., Ru(bpy)₃], accounting for the potential for charge neutralization on the surface. We found that neutral Configuration 1 is also more energetically stable (by 0.66 eV) than neutral Configuration 2. Consequently, Configuration 1 is designated as the adsorption geometry of the Ru(bpy)₃ molecules (in their charged or neutral state) on the Cu(100) surface. Following the configuration assignment, we computed the non-resonance Raman spectra of Ru(bpy)₃²⁺ and Ru(bpy)₃ for Configuration 1 based on TDDFT calculations and compared them to the TERS measurements. The simulated spectra were divided into x-, y-, and z-components (as shown in Supporting Information, Figure S5), and we compared the out-of-plane vibrational

modes (z-components) of Configuration 1 [charged (+2) and neutral species] with the experimental TERS spectrum based on the expected effects of the selection rules of TERS (Supporting Information, Figure S6).⁷⁹

Figure 3b illustrates the comparison between the experimental TERS and simulated Raman spectra of Ru(bpy)₃²⁺ [pink spectrum (z-axis)] and Ru(bpy)₃ [blue spectrum (z-axis)]. Let us first analyze the influence of charge on the molecular structure and how it impacts the Raman spectra (i.e., pink and blue spectra). While the spectral characteristics are more or less similar, there are discernible differences in the case of charge neutralization (i.e., the transition from the charged state to the neutral state), as indicated by green dotted rectangles. To begin with, the pink spectrum's two peaks in the 1600 cm⁻¹ to 1500 cm⁻¹ range have been altered to three distinct peaks (blue spectrum), which correspond to C-C stretching and C-H wagging modes of 2,2'bipyridine functional groups⁷² (Supporting Information, Figure S7). Secondly, the peak located in the ~1300 cm⁻¹ region (consisting of 2-2' C—C stretching, C—H wagging, C—C, and C—N stretching modes)⁷² has been divided into a doublet of two equally intense peaks (Supporting Information, Figure S7). Lastly, a prominent peak is observed in the ~1100 cm⁻¹ region for the neutral species, dominated by the vibrations of 2,2'-bipyridine structure. Subsequently, the experimental TERS spectrum (red spectrum) is aligned with the simulated Raman spectra (Figure 3b). A reasonable agreement between the DFT simulations and the experimental TERS is achieved for the charged-Ru(bpy)₃ molecule [Ru(bpy)₃²⁺, pink spectrum], where the spectral profile and the majority of the prominent peaks exhibit a close resemblance. It is noteworthy that in the experiment, some peaks, especially in the region of 1600 cm⁻¹ to 1400 cm⁻¹, exhibit a minor shift, which could be attributed to the interactions between the tip and the molecule during spectra acquisition (as the tip was approached close to the molecule). Such interactions may cause a "weak" physical interaction that may perturb the adsorption geometry (slightly) of the Ru(bpy)₃²⁺ molecule. ⁸⁰ Based on the DFT and TDDFT simulations and the single-molecule TERS characterization, we can confirm that the molecules on the Cu(100) surface remain in their charged state [i.e., Ru(bpy)₃²⁺] and do not undergo charge neutralization into the surface. The negligible charge transfer (as simulated from DFT, Supporting Information, Figure S8) between the Ru(II) metal core and the underlying Cu surface, as shown in Figure 3a, further supports this conclusion. The biphenyl groups lift the charged Ru core (Ru²⁺) by approximately 0.63 nm away from the Cu surface (Figure 3a) which most likely hinders the charge transfer (i.e., decoupling from the metal surface), thereby stabilizing the charged species directly on the metal surface. ³⁸ Therefore, the STM-combined TERS technique allows for the identification of detailed information regarding the three-dimensional binding configuration of the octahedrally coordinated complex molecule and the recognition of its charged state on the surface.

What remains to be discussed is the formation of molecular dimers and surface aggregation of Ru(bpy)₃²⁺ molecules over the Cu(100) surface. We consider dipole-dipole coupling interactions as the possible reason for the dimer formation.⁸¹ In the gas phase, the structure of the molecule is symmetric (D₃ point group), so the dipole moment is negligible. However, when absorbed on the surface, the dipole moment of charged-Ru(bpy)₃ [Ru(bpy)₃²⁺] is calculated to be 0.15 D (in the X-direction, Figure 4a), parallel to the Cu surface. As the charge transfer between the molecule and surface remains negligible, the induced dipole is due to structural deformation (which breaks the symmetry) upon adsorption on the surface. The presence of a non-zero dipole moment parallel to the surface could allow for various ways for two monomers to interact with each other, depending on the molecular rotation around the Z-axis. The dipole-

dipole coupling strength can be represented by |J|, where within point-dipole approximation, J can be simply expressed as:⁸²

$$J \approx \frac{\mu_1 \cdot \mu_2}{4\pi\varepsilon_0 d^3}$$

where μ_1 and μ_2 are the dipole moments (with amplitude μ_0) of the component monomers, d is the position vector (intermolecular distance) between two monomers, and ε_0 is the permittivity in the vacuum.

As mentioned, each Ru(bpy) $_3^{2+}$ molecule possesses a nonzero dipole moment in the X-direction (parallel to the surface). Consequently, there are five possible ways that each dipole can interact with each other (considering molecular rotation around Z-axis) to form a molecular dimer: in-line in-phase $[(\to\to)$, Type 1], parallel out-of-phase $[(\downarrow\uparrow)$, Type 2], orthogonal $[(\uparrow\to \text{and} \to\uparrow)$, Type 3], parallel in-phase $[(\uparrow\uparrow)$, Type 4], and in-line out-of-phase $[(\to\leftarrow)$, Type 5], as shown in Figure 4b.⁸² The associated J for different dipole phase relations is:

$$J_{\to\to} = -\frac{2\mu_0^2}{4\pi d^3} = -J_{\to\leftarrow}$$
, $J_{\downarrow\uparrow} = -\frac{\mu_0^2}{4\pi d^3} = -J_{\uparrow\uparrow}$, and $J_{\uparrow\to} = 0 = J_{\to\uparrow}$

Using the coupling strength predicted by the equation mentioned above, we determined the energy levels (shown in Figure 4c) and found that Type 1 (i.e., in-line in-phase coupling) has the lowest energy. This indicates that in-line in-phase coupling is the most energetically favorable way for the two monomers to interact, leading to the formation of the observed molecular dimers (as depicted in Figure 4b), which is consistent with our STM observations (Figures 1b–d). Therefore, we propose that the observed molecular dimers on Cu(100) result from Type 1 dipole-dipole coupling interactions (as assigned in the Supporting Information, Figure S9). The strength of dipole-dipole coupling increases with decreasing intermolecular distances, (i.e., $J \rightarrow \infty = \frac{1}{d^3}$), so we

suggest that the formation of molecular dimers involves a delicate balance between attractive dipole-dipole interactions (which depend on the intermolecular distances) and electrostatic repulsions (due to the positive charges of the molecules). Along with the dipole-dipole attractive interactions, the alignment of dimer aggregation relative to the crystallographic direction of the Cu(100) surface indicates that the surface lattice plays a crucial role in guiding the orientation and spacing of the molecular aggregates. Hence, the combination of these various factors results in an average intermolecular distance of $\sim 1.01 \pm 0.04$ nm for most of the dimers (as seen in Figures 1a– d). Moreover, at a slightly larger intermolecular distance (e.g., ~1.35 nm, as in Figure 1d), the strength of "in-line in-phase" coupling weakens, causing the individual molecules to deviate slightly from their parallel position. Moreover, these dipole-dipole coupling interactions can result in linear arrays of molecules on the surface, as illustrated in the Supporting Information (Figure S10). Following this investigation of Ru(bpy)₃²⁺ molecules on the Cu(100) surface, future work will focus on one-electron oxidation and reduction reactions [i.e., Ru(bpy)₃³⁺ and Ru(bpy)₃⁺ respectively] on surfaces, in which redox reactions and spectroscopic measurements will be performed.

4. Conclusion

In conclusion, the charged state, adsorption configuration, as well as surface aggregation of Ru(bpy)₃²⁺ molecules over Cu(100) surface have been explored by STM-TERS in combination with (TD)DFT calculations. Based on the STM images, molecular dimers are identified. However, the charge states of the molecules remain ambiguous. Finally, the chemical fingerprints attained using TERS display a crucial sensitivity to charge states and binding configurations, confirming that the Ru(bpy)₃²⁺ molecule remains in the charged (+2) state on the Cu(100) surface. The agreement between the experimental and simulated Raman spectra suggests negligible charge

transfer between the molecule and Cu(100) surface, which is further complemented through DFT simulations. Moreover, the potential formation of molecular dimers can be theorized through dipole-dipole attractive interactions, facilitated by the creation of a dipole moment (in-plane) upon adsorption. For charged organic molecules, understanding their surface aggregation over a solid surface requires characterizing local chemical effects at the atomic scale. STM-TERS emerges as an excellent tool for probing the charged state, adsorbed configuration, and surface aggregation of these organic molecular structures, holding significance for next-generation organic device fabrication.

ASSOCIATED CONTENT

Supporting Information

Zoom-in STM image and Ball-and-Stick model of Ru(bpy) $_3^{2+}$ molecule; STM image and STM height profile of molecular dimers; DFT simulated possible configurations of Ru(bpy) $_3^{2+}$ molecule (Configuration 1 and 2) on the Cu(100) surface; STM images before and after TERS measurements; Simulated non-resonance Raman spectra of charged- and neutral-Ru(bpy) $_3$ molecule for Configuration 1 on the Cu(100) surface in x-, y-, and z-direction; Schematic illustration of TERS selection rules; Simulation of vibrational modes for charged- and neutral-Ru(bpy) $_3$ molecule for selected peaks (Configuration 1); Charge density measurements of ρ [Ru(bpy) $_3^{2+}$ +Cu]; STM image and schematic representation of "in-line in-phase" dipole-dipole interaction; STM image of four Ru(bpy) $_3^{2+}$ molecules (nano-arrays); Powder Raman spectrum of $C_{30}H_{24}Cl_2N_6Ru \cdot 6H_2O$.

Author Information

Corresponding Author

*E-mail: njiang@uic.edu

ORCID

Sayantan Mahapatra: 0000-0002-7332-196X

Chamath Siribaddana: 0000-0001-6331-4945

Linfei Li: 0000-0002-5217-3005

Soumyajit Rajak: 0009-0000-0881-2431

Xu Zhang: 0000-0002-6491-3234

Nan Jiang: 0000-0002-4570-180X

Notes

The authors declare no competing financial interest.

ACKNOWLEDGMENTS

N.J. acknowledges support from the National Science Foundation (CHE-1944796). X.Z. acknowledges support from the National Science Foundation (DMR-1828019).

REFERENCES

- Grunder, Y.; Lucas, C. A.; Thompson, P. B. J.; Joly, Y.; Soldo-Olivier, Y., Charge Reorganization at the Adsorbate Covered Electrode Surface Probed through in Situ Resonant X-Ray Diffraction Combined with Ab Initio Modeling. *J. Phys. Chem. C* 2022, *126*, 4612-4619.
- Fernández-Torrente, I.; Franke, K. J.; Pascual, J. I., Vibrational Kondo Effect in Pure Organic Charge-Transfer Assemblies. *Phys. Rev. Lett.* 2008, 101, 217203.
- 3. Pireddu, G.; Scalfi, L.; Rotenberg, B., A Molecular Perspective on Induced Charges on a Metallic Surface. *J. Chem. Phys.* **2021**, *155*, 204705.
- Repp, J.; Meyer, G.; Stojković, S. M.; Gourdon, A.; Joachim, C., Molecules on Insulating Films: Scanning-Tunneling Microscopy Imaging of Individual Molecular Orbitals. *Phys. Rev. Lett.* 2005, 94, 026803.
- 5. Binnig, G.; Rohrer, H., Scanning Tunneling Microscopy. Surf. Sci. 1983, 126, 236-244.
- Swart, I.; Sonnleitner, T.; Repp, J., Charge State Control of Molecules Reveals Modification of the Tunneling Barrier with Intramolecular Contrast. *Nano Lett.* 2011, 11, 1580-1584.
- Kaiser, K.; Lieske, L.-A.; Repp, J.; Gross, L., Charge-State Lifetimes of Single Molecules on Few Monolayers of Nacl. *Nat. Commun.* 2023, 14, 4988.
- 8. Mahapatra, S.; Li, L.; Schultz, J. F.; Jiang, N., Tip-Enhanced Raman Spectroscopy: Chemical Analysis with Nanoscale to Angstrom Scale Resolution. *J. Chem. Phys.* **2020**, *153*, 010902.
- 9. Schultz, J. F.; Mahapatra, S.; Li, L.; Jiang, N., The Expanding Frontiers of Tip-Enhanced Raman Spectroscopy. *Appl. Spectrosc.* **2020**, *74*, 1313-1340.
- Verma, P., Tip-Enhanced Raman Spectroscopy: Technique and Recent Advances. *Chem. Rev.* 2017, 117, 6447-6466.
- 11. Pozzi, E. A.; Goubert, G.; Chiang, N.; Jiang, N.; Chapman, C. T.; McAnally, M. O.; Henry, A-I.; Seideman, T.; Schatz, G. C.; Hersam, M. C.; Van Duyne, R. P., Ultrahigh-Vacuum Tip-Enhanced Raman Spectroscopy. *Chem. Rev.* **2017**, *117*, 4961-4982.
- 12. Jiang, N.; Foley, E. T.; Klingsporn, J. M.; Sonntag, M. D.; Valley, N. A.; Dieringer, J. A.; Seideman, T.; Schatz, G. C.; Hersam, M. C.; Van Duyne, R. P., Observation of Multiple Vibrational

- Modes in Ultrahigh Vacuum Tip-Enhanced Raman Spectroscopy Combined with Molecular-Resolution Scanning Tunneling Microscopy. *Nano Lett.* **2012**, *12*, 5061-5067.
- Jiang, N.; Kurouski, D.; Pozzi, E. A.; Chiang, N.; Hersam, M. C.; Van Duyne, R. P., Tip-Enhanced
 Raman Spectroscopy: From Concepts to Practical Applications. *Chem. Phys. Lett.* 2016, 659, 16-24.
- Zhang, R.; Zhang, Y.; Dong, Z. C.; Jiang, S.; Zhang, C.; Chen, L. G.; Zhang, L.; Liao, Y.; Azipurua,
 J.; Luo, Y., et al., Chemical Mapping of a Single Molecule by Plasmon-Enhanced Raman
 Scattering. Nature 2013, 498, 82-86.
- 15. El-Khoury, P. Z., Tip-Enhanced Raman Scattering on Both Sides of the Schrödinger Equation. *Acc. Chem. Res.* **2021**, *54*, 4576-4583.
- 16. El-Khoury, P. Z.; Schultz, Z. D., From SERS to TERS and Beyond: Molecules as Probes of Nanoscopic Optical Fields. *J. Phys. Chem. C* **2020**, *124*, 27267-27275.
- 17. Schultz, J. F., Tip-Enhanced Raman Scattering for Atomic-Scale Spectroscopy and Imaging. *Nat. Rev. Phys.* **2023**, *5*, 5-5.
- 18. Sonntag, M. D.; Pozzi, E. A.; Jiang, N.; Hersam, M. C.; Van Duyne, R. P., Recent Advances in Tip-Enhanced Raman Spectroscopy. *J. Phys. Chem. Lett.* **2014**, *5*, 3125-3130.
- 19. Mahapatra, S.; Liu, D.; Siribaddana, C.; Wang, K.; Li, L.; Jiang, N., Localized Surface Plasmon Controlled Chemistry at and Beyond the Nanoscale. *Chem. Phys. Rev.* **2023**, *4*, 021301.
- 20. Paulite, M.; Blum, C.; Schmid, T.; Opilik, L.; Eyer, K.; Walker, G. C.; Zenobi, R., Full Spectroscopic Tip-Enhanced Raman Imaging of Single Nanotapes Formed from β-Amyloid(1–40) Peptide Fragments. *ACS Nano* **2013**, *7*, 911-920.
- 21. Helbing, C.; Deckert-Gaudig, T.; Firkowska-Boden, I.; Wei, G.; Deckert, V.; Jandt, K. D., Protein Handshake on the Nanoscale: How Albumin and Hemoglobin Self-Assemble into Nanohybrid Fibers. *ACS Nano* **2018**, *12*, 1211-1219.
- 22. Alexander, K. D.; Schultz, Z. D., Tip-Enhanced Raman Detection of Antibody Conjugated Nanoparticles on Cellular Membranes. *Anal. Chem.* **2012**, *84*, 7408-7414.

- 23. Wang, H.; Schultz, Z. D., Ters Detection of Avβ3 Integrins in Intact Cell Membranes.

 ChemPhysChem 2014, 15, 3944-3949.
- 24. Kradolfer, S.; Lipiec, E.; Baldacchini, C.; Bizzarri, A. R.; Cannistraro, S.; Zenobi, R., Vibrational Changes Induced by Electron Transfer in Surface Bound Azurin Metalloprotein Studied by Tip-Enhanced Raman Spectroscopy and Scanning Tunneling Microscopy. ACS Nano 2017, 11, 12824-12831.
- Zhang, R.; Zhang, X.; Wang, H.; Zhang, Y.; Jiang, S.; Hu, C.; Zhang, Y.; Luo, Y.; Dong, Z., Distinguishing Individual DNA Bases in a Network by Non-Resonant Tip-Enhanced Raman Scattering. Angew. Chem. Int. Ed. 2017, 56, 5561.
- Sheng, S.; Wu, J.-b.; Cong, X.; Li, W.; Gou, J.; Zhong, Q.; Cheng, P.; Tan, P.-h.; Chen, L.; Wu,
 K., Vibrational Properties of a Monolayer Silicene Sheet Studied by Tip-Enhanced Raman
 Spectroscopy. *Phys. Rev. Lett.* 2017, 119, 196803.
- Sheng, S.; Wu, J-B.; Cong, X.; Zhong, Q.; Li, W.; Hu, W.; Gou, J.; Cheng, P.; Tan, P-H.; Chen,
 L.; Wu, K., Raman Spectroscopy of Two-Dimensional Borophene Sheets. ACS Nano 2019, 13,
 4133-4139.
- Zhang, H-T., Park, T. J.; Nafiul Islam, A. N. M.; Tran, D. S. J.; Manna, S.; Wang, Q.; Mondal, S.; Yu, H.; Bank, S., Cheng, S., et al., Reconfigurable Perovskite Nickelate Electronics for Artificial Intelligence. Science 2022, 375, 533-539.
- Liu, D.; Li, L.; Jiang, N., Nanoscale Chemical Probing of Metal-Supported Ultrathin Ferrous Oxide
 Via Tip-Enhanced Raman Spectroscopy and Scanning Tunneling Microscopy. *Chem. Biomed. Imaging* 2024, 2, 345-351.
- 30. Schultz, J. F.; Jiang, N., Characterizations of Two-Dimensional Materials with Cryogenic Ultrahigh Vacuum near-Field Optical Microscopy in the Visible Range. *J. Vac. Sci. Technol. A* **2022**, *40*, 040801.

- 31. Shao, F.; Wang, W.; Yang, W.; Yang, Z.; Zhang, Y.; Lan, J.; Dieter Schlüter, A.; Zenobi, R., In-Situ Nanospectroscopic Imaging of Plasmon-Induced Two-Dimensional [4+4]-Cycloaddition Polymerization on Au(111). *Nat. Commun.* **2021**, *12*, 4557.
- 32. Shao, F.; Dai, W.; Zhang, Y.; Zhang, W.; Schlüter, A. D.; Zenobi, R., Chemical Mapping of Nanodefects within 2d Covalent Monolayers by Tip-Enhanced Raman Spectroscopy. *ACS Nano* **2018**, *12*, 5021-5029.
- 33. Zhong, J.-H.; Jin, X.; Meng, L.; Wang, X.; Su, H.-S.; Yang, Z.-L.; Williams, C. T.; Ren, B., Probing the Electronic and Catalytic Properties of a Bimetallic Surface with 3 nm Resolution. *Nat. Nanotechnol.* **2017**, *12*, 132-136.
- 34. Schultz, J. F.; Li, L.; Mahapatra, S.; Jiang, N., Chemically Imaging Nanostructures Formed by the Covalent Assembly of Molecular Building Blocks on a Surface with Ultrahigh Vacuum Tip-Enhanced Raman Spectroscopy. *J. Condens. Matter Phys.* **2022**, *34*, 204008.
- van Schrojenstein Lantman, E. M.; Deckert-Gaudig, T.; Mank, A. J. G.; Deckert, V.; Weckhuysen,
 B. M., Catalytic Processes Monitored at the Nanoscale with Tip-Enhanced Raman Spectroscopy.
 Nat. Nanotechnol. 2012, 7, 583-586.
- 36. Mahapatra, S.; Schultz, J. F.; Li, L.; Zhang, X.; Jiang, N., Controlling Localized Plasmons Via an Atomistic Approach: Attainment of Site-Selective Activation inside a Single Molecule. *J. Am. Chem. Soc.* **2022**, *144*, 2051-2055.
- Chiang, N., Chen, X.; Goubert, G.; Chulhai, D. V.; Chen, X.; Pozzi, E. A., Jiang, N.; Hersam, M.
 C.; Seideman, T.; Jensen, L.; Van Duyne, R. P., Conformational Contrast of Surface-Mediated Molecular Switches Yields Ångstrom-Scale Spatial Resolution in Ultrahigh Vacuum Tip-Enhanced Raman Spectroscopy. *Nano Lett.* 2016, 16, 7774-7778.
- 38. Chiang, N.; Jiang, N.; Chulhai, D. V.; Pozzi, E. A.; Hersam, M. C.; Jensen, L.; Seideman, T.; Van Duyne, R. P., Molecular-Resolution Interrogation of a Porphyrin Monolayer by Ultrahigh Vacuum Tip-Enhanced Raman and Fluorescence Spectroscopy. *Nano Lett.* **2015**, *15*, 4114-4120.

- Chiang, N.; Jiang, N.; Madison, L. R.; Pozzi, E. A.; Wasielewski, M. R.; Ratner, M. A.; Hersam,
 M. C.; Seideman, T.; Schatz, G. C.; Van Duyne, R. P., Probing Intermolecular Vibrational
 Symmetry Breaking in Self-Assembled Monolayers with Ultrahigh Vacuum Tip-Enhanced Raman
 Spectroscopy. J. Am. Chem. Soc. 2017, 139, 18664-18669.
- 40. Schultz, J. F.; Li, L.; Mahapatra, S.; Shaw, C.; Zhang, X.; Jiang, N., Defining Multiple Configurations of Rubrene on a Ag(100) Surface with 5 Å Spatial Resolution Via Ultrahigh Vacuum Tip-Enhanced Raman Spectroscopy. *J. Phys. Chem. C* **2020**, *124*, 2420-2426.
- 41. Mahapatra, S.; Schultz, J. F.; Li, L.; Zhang, X.; Jiang, N., Chemical Characterization of a Three-Dimensional Double-Decker Molecule on a Surface Via Scanning-Tunneling-Microscopy-Based Tip-Enhanced Raman Spectroscopy. *J. Phys. Chem. C* **2022**, *126*, 8734-8741.
- 42. Mahapatra, S.; Schultz, J. F.; Ning, Y.; Zhang, J.-L.; Jiang, N., Probing Surface Mediated Configurations of Nonplanar Regioisomeric Adsorbates Using Ultrahigh Vacuum Tip-Enhanced Raman Spectroscopy. *Nanoscale* **2019**, *11*, 19877-19883.
- 43. Bhattarai, A.; Joly, A. G.; Hess, W. P.; El-Khoury, P. Z., Visualizing Electric Fields at Au(111) Step Edges Via Tip-Enhanced Raman Scattering. *Nano Lett.* **2017**, *17*, 7131-7137.
- 44. Li, L.; Mahapatra, S.; Liu, D.; Lu, Z.; Jiang, N., On-Surface Synthesis and Molecular Engineering of Carbon-Based Nanoarchitectures. *ACS Nano* **2021**, *15*, 3578-3585.
- 45. Xiaoru, D.; Ben, Y.; Rui, Z.; Ruipu, W.; Yang, Z.; Yao, Z.; Zhenchao, D., Tip-Induced Bond Weakening, Tilting, and Hopping of a Single Co Molecule on Cu(100). *Light Adv. Manuf.* **2022**, *3*, 1-10.
- 46. Zhang, Y.; Yang, B.; Ghafoor, A.; Zhang, Y.; Zhang, Y.-F.; Wang, R.-P.; Yang, J.-L.; Luo, Y.; Dong, Z.-C.; Hou, J. G., Visually Constructing the Chemical Structure of a Single Molecule by Scanning Raman Picoscopy. *Natl. Sci. Rev.* 2019, 6, 1169-1175.
- 47. Jaculbia, R. B.; Imada, H.; Miwa, K.; Iwasa, T.; Takenaka, M.; Yang, B.; Kazuma, E.; Hayazawa, N.; Taketsugu, T.; Kim, Y., Single-Molecule Resonance Raman Effect in a Plasmonic Nanocavity.

 Nat. Nanotechnol. 2020, 15, 105-110.

- 48. Xu, J., Zhu, X.; Tan, S.; Zhang, Y.; Li, B.; Tian, Y.; Shan, H.; Cui, X.; Zhao, A.; Dong, Z-C., et al., Determining Structural and Chemical Heterogeneities of Surface Species at the Single-Bond Limit. Science 2021, 371, 818-822.
- 49. Mahapatra, S.; Jiang, N., Precise Tracking of Tip-Induced Structural Variation at the Single-Chemical-Bond Limit. *Light Sci. Appl.* **2023**, *12*, 21.
- 50. Tallarida, N.; Lee, J.; Apkarian, V. A., Tip-Enhanced Raman Spectromicroscopy on the Angstrom Scale: Bare and Co-Terminated Ag Tips. *ACS Nano* **2017**, *11*, 11393-11401.
- 51. Gleria, M.; Minto, F.; Beggiato, G.; Bortolus, P., Photochemistry of Tris(2,2'-Bipyridine)Ruthenium(Ii) in Chlorinated Solvents. *J. Chem. Soc., Chem. Commun.* **1978**, 285a-285a.
- 52. White, H. S.; Becker, W. G.; Bard, A. J., Photochemistry of the Tris(2,2'-Bipyridine)Ruthenium(Ii)-Peroxydisulfate System in Aqueous and Mixed Acetonitrile-Water Solutions. Evidence for a Long-Lived Photoexcited Ion Pair. J. Phys. Chem. 1984, 88, 1840-1846.
- 53. Stacy, A. A.; Van Duyne, R. P., Surface Enhanced Raman and Resonance Raman Spectroscopy in a Non-Aqueous Electrochemical Environment: Tris(2,2'-Bipyridine)Ruthenium(II) Adsorbed on Silver from Acetonitrile. *Chem. Phys. Lett.* **1983**, *102*, 365-370.
- 54. Elliott, C. M.; Freitag, R. A.; Blaney, D. D., Electrochemistry, Spectroelectrochemistry, and Photochemistry of a Series of New Covalently Linked Tris(2,2-Bipyridine)Ruthenium(II)/Diquat Complexes. J. Am. Chem. Soc. 1985, 107, 4647-4655.
- 55. Yoon, T. P.; Ischay, M. A.; Du, J., Visible Light Photocatalysis as a Greener Approach to Photochemical Synthesis. *Nat. Chem.* **2010**, *2*, 527-532.
- 56. Soltzberg, L. J.; Slinker, J. D.; Flores-Torres, S.; Bernards, D. A.; Malliaras, G. G.; Abruña, H. D.; Kim, J.-S.; Friend, R. H.; Kaplan, M. D.; Goldberg, V., Identification of a Quenching Species in Ruthenium Tris-Bipyridine Electroluminescent Devices. J. Am. Chem. Soc. 2006, 128, 7761-7764.
- 57. O'Regan, B.; Grätzel, M., A Low-Cost, High-Efficiency Solar Cell Based on Dye-Sensitized Colloidal TiO₂ Films. *Nature* **1991**, *353*, 737-740.

- 58. Edward Van, K.; David, L.; Wolfgang, S., Three-Dimensional Thermal Imaging Using Two-Photon Microscopy. *Journal of Physics D: Appl. Phys.* **2004**, *37*, 2938.
- 59. Ceroni, P.; Bergamini, G.; Balzani, V., Old Molecules, New Concepts: [Ru(Bpy)₃]²⁺ as a Molecular Encoder–Decoder. *Angew. Chem. Intl. Ed.* **2009**, *48*, 8516-8518.
- 60. Bunjes, O.; Hedman, D.; Rittmeier, A.; Paul, L. A.; Siewert, I.; Ding, F.; Wenderoth, M., Making and Breaking of Chemical Bonds in Single Nanoconfined Molecules. *Sci. Adv.*, 8, eabq7776.
- Zhao, J.; Dieringer, J. A.; Zhang, X.; Schatz, G. C.; Van Duyne, R. P., Wavelength-Scanned Surface-Enhanced Resonance Raman Excitation Spectroscopy. J. Phys. Chem. C 2008, 112, 19302-19310.
- 62. Klingsporn, J. M.; Jiang, N.; Pozzi, E. A.; Sonntag, M. D.; Chulhai, D.; Seideman, T.; Jensen, L.; Hersam, M. C.; Duyne, R. P. V., Intramolecular Insight into Adsorbate–Substrate Interactions Via Low-Temperature, Ultrahigh-Vacuum Tip-Enhanced Raman Spectroscopy. *J. Am. Chem. Soc.* 2014, 136, 3881-3887.
- 63. Mahapatra, S.; Li, L.; Schultz, J. F.; Jiang, N., Methods to Fabricate and Recycle Plasmonic Probes for Ultrahigh Vacuum Scanning Tunneling Microscopy-Based Tip-Enhanced Raman Spectroscopy. *J. Raman Spectrosc.* **2021**, *52*, 573-580.
- 64. Whiteman, P. J.; Schultz, J. F.; Porach, Z. D.; Chen, H.; Jiang, N., Dual Binding Configurations of Subphthalocyanine on Ag(100) Substrate Characterized by Scanning Tunneling Microscopy, Tip-Enhanced Raman Spectroscopy, and Density Functional Theory. J. Phys. Chem. C 2018, 122, 5489-5495.
- 65. Kresse, G.; Furthmüller, J., Efficient Iterative Schemes for Ab Initio Total-Energy Calculations Using a Plane-Wave Basis Set. *Phys. Rev. B* **1996**, *54*, 11169-11186.
- 66. Blöchl, P. E., Projector Augmented-Wave Method. *Phys. Rev. B* **1994**, *50*, 17953-17979.
- 67. Perdew, J. P.; Burke, K.; Ernzerhof, M., Generalized Gradient Approximation Made Simple. *Phys. Rev. Lett.* **1996**, *77*, 3865-3868.

- 68. Dion, M.; Rydberg, H.; Schröder, E.; Langreth, D. C.; Lundqvist, B. I., Van Der Waals Density Functional for General Geometries. *Phys. Rev. Lett.* **2004**, *92*, 246401.
- 69. Baroni, S.; de Gironcoli, S.; Dal Corso, A.; Giannozzi, P., Phonons and Related Crystal Properties from Density-Functional Perturbation Theory. *Rev. Mod. Phys.* **2001**, *73*, 515-562.
- 70. Zhang, X., Large-Scale Ab Initio Calculations of Raman Scattering Spectra within Time-Dependent Density Functional Perturbation Theory. *J. Chem. Phys.* **2018**, *148*, 244103.
- 71. Johnson, G. E.; Lysonski, M.; Laskin, J., In Situ Reactivity and Tof-Sims Analysis of Surfaces Prepared by Soft and Reactive Landing of Mass-Selected Ions. *Anal. Chem.* **2010**, *82*, 5718-5727.
- 72. Silverstein, D. W.; Milojevich, C. B.; Camden, J. P.; Jensen, L., Investigation of Linear and Nonlinear Raman Scattering for Isotopologues of Ru(Bpy)₃²⁺. *J. Phys. Chem. C* **2013**, *117*, 20855-20866.
- 73. Lee, J.; Crampton, K. T.; Tallarida, N.; Apkarian, V. A., Visualizing Vibrational Normal Modes of a Single Molecule with Atomically Confined Light. *Nature* **2019**, *568*, 78-82.
- Mannix, A. J., Zhou, X-F.; Kiraly, B.; Wood, J. D.; Alducin, D.; Myers, B, D.; Liu, X., Fisher, B.
 L., Santiago, U.; Guest, J. R., et al., Synthesis of Borophenes: Anisotropic, Two-Dimensional Boron Polymorphs. Science 2015, 350, 1513-1516.
- 75. Li, L.; Schultz, J. F.; Mahapatra, S.; Liu, X.; Zhang, X.; Hersam, M. C.; Jiang, N., Atomic-Scale Insights into the Interlayer Characteristics and Oxygen Reactivity of Bilayer Borophene. *Angew. Chem. Intl. Ed.* 2023, 62, e202306590.
- Li, L.; Schultz, J. F.; Mahapatra, S.; Liu, X.; Shaw, C.; Zhang, X.; Hersam, M. C.; Jiang, N.,
 Angstrom-Scale Spectroscopic Visualization of Interfacial Interactions in an Organic/Borophene
 Vertical Heterostructure. J. Am. Chem. Soc. 2021, 143, 15624-15634.
- 77. Li, L.; Schultz, J. F.; Mahapatra, S.; Lu, Z.; Zhang, X.; Jiang, N., Chemically Identifying Single Adatoms with Single-Bond Sensitivity During Oxidation Reactions of Borophene. *Nat. Commun.* **2022**, *13*, 1796.

- 78. Mahapatra, S.; Ning, Y.; Schultz, J. F.; Li, L.; Zhang, J.-L.; Jiang, N., Angstrom Scale Chemical Analysis of Metal Supported Trans- and Cis-Regioisomers by Ultrahigh Vacuum Tip-Enhanced Raman Mapping. *Nano Lett.* **2019**, *19*, 3267-3272.
- 79. Jiang, N.; Chiang, N.; Madison, L. R.; Pozzi, E. A.; Wasielewski, M. R.; Seideman, T.; Ratner, M. A.; Hersam, M. C.; Schatz, G. C.; Van Duyne, R. P., Nanoscale Chemical Imaging of a Dynamic Molecular Phase Boundary with Ultrahigh Vacuum Tip-Enhanced Raman Spectroscopy. *Nano Lett.* 2016, 16, 3898-3904.
- 80. Yang, B.; Chen, G.; Ghafoor, A.; Zhang, Y-F.; Zhang, X-B., Li, H.; Dong, X-R.; Wang, R-P.; Zhang, Y.; Zhang, Y.; Dong, Z-C., Chemical Enhancement and Quenching in Single-Molecule Tip-Enhanced Raman Spectroscopy. *Angew. Chem. Intl. Ed.* **2023**, *62*, e202218799.
- 81. Jiang, N.; Zhang, Y. Y.; Liu, Q.; Cheng, Z. H.; Deng, Z. T.; Du, S. X.; Gao, H. J.; Beck, M. J.; Pantelides, S. T., Diffusivity Control in Molecule-on-Metal Systems Using Electric Fields. *Nano Lett.* **2010**, *10*, 1184-1188.
- 82. Zhang, Y.; Luo, Y.; Zhang, Y.; Yu, Y-J.; Kuang, Y-M.; Zhang, L.; Meng, Q-S.; Luo, Y.; Yang, J-L.; Dong, Z-C.; Hou, J. G., Visualizing Coherent Intermolecular Dipole–Dipole Coupling in Real Space. *Nature* 2016, 531, 623-627.

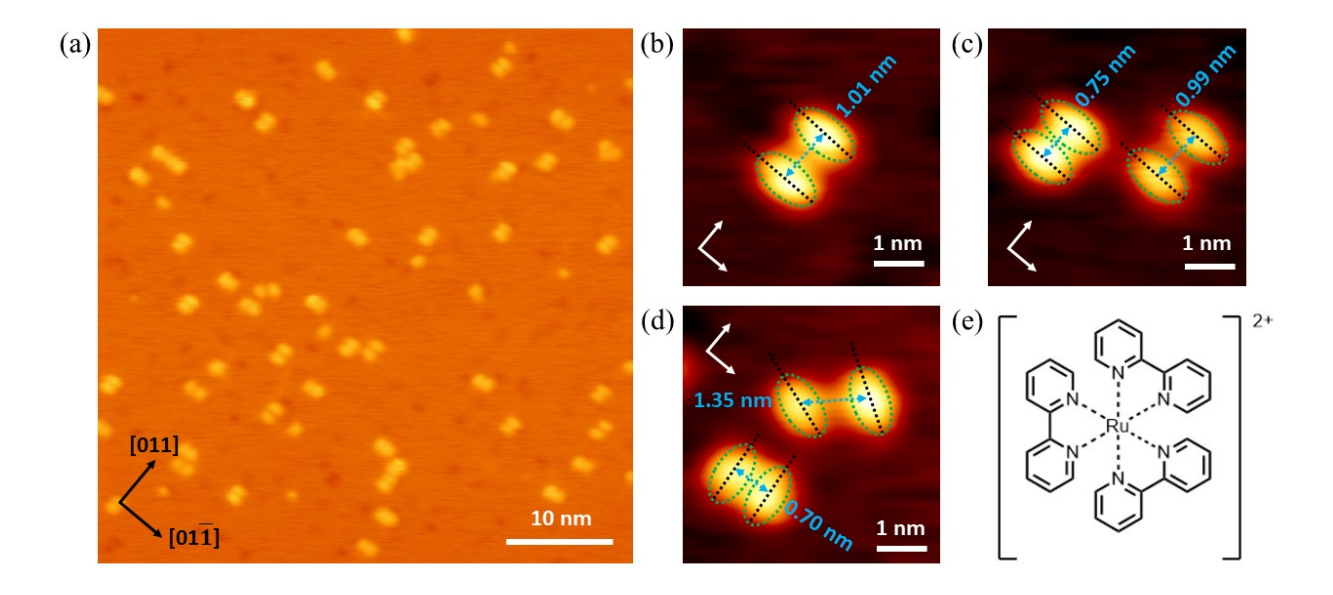


Figure 1. (a) Large-scale constant-current STM image of Ru(bpy) $_3^{2+}$ molecules on the Cu(100) surface. (b–d) Zoom-in STM images of molecular dimers with different intermolecular distances [center to center, ranging from 1.35 nm to 0.70 nm]. The ellipsoidal shape of the molecule was identified by green dotted ellipsoids. Crystallographic directions are identified. For (b–d), the lattice direction is identical to (a). STM conditions: $I_t = 1$ nA and V = 1.0 V. (e) Chemical structure of Ru(bpy) $_3^{2+}$.

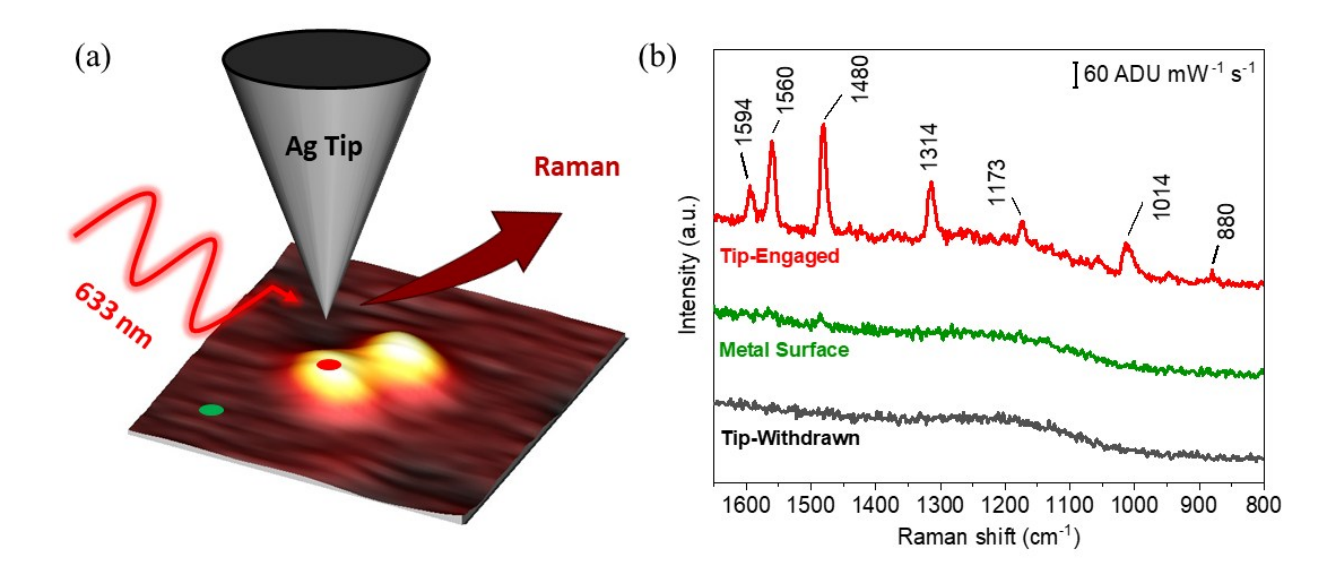


Figure 2. (a) Schematic illustration of TERS on Ru(bpy)₃²⁺ molecules on the Cu(100) surface. A 633 nm laser excitation was utilized. (b) TERS fingerprint (red) of a Ru(bpy)₃²⁺ molecule acquired when the tip is parked (and engaged) over the red spot in (a). The tip-engaged spectrum over the metal surface (green) and the tip-withdrawn spectrum (black) are featureless. TERS conditions: It = 4 nA, V = 0.1 V, λ_{ex} = 633 nm, P_{acq} = 0.5 mW, t_{acq} = 10 s.

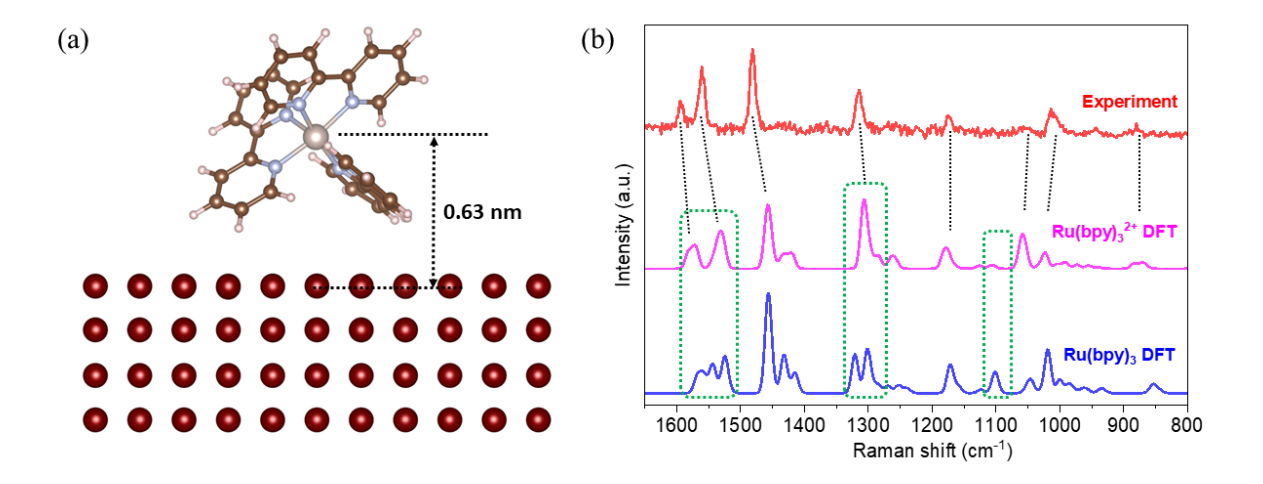


Figure 3. (a) DFT optimized structure (Configuration 1) of Ru(bpy)₃²⁺ molecules on the Cu(100) surface. The Ru(II) center stays 0.63 nm away from the Cu surface. (b) Comparison between simulated TERS (z-direction) for Ru(bpy)₃²⁺ (pink spectrum) and Ru(bpy)₃ (blue spectrum) molecule [adsorbed on Cu(100)] and experimental TERS (red spectrum).

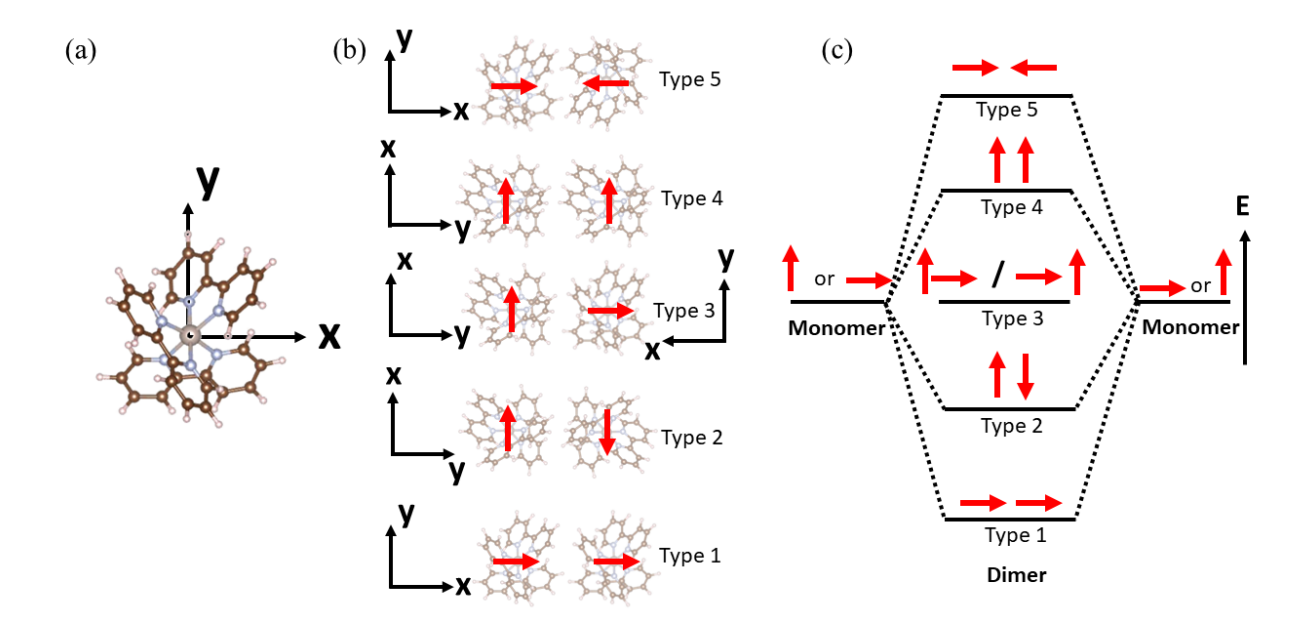
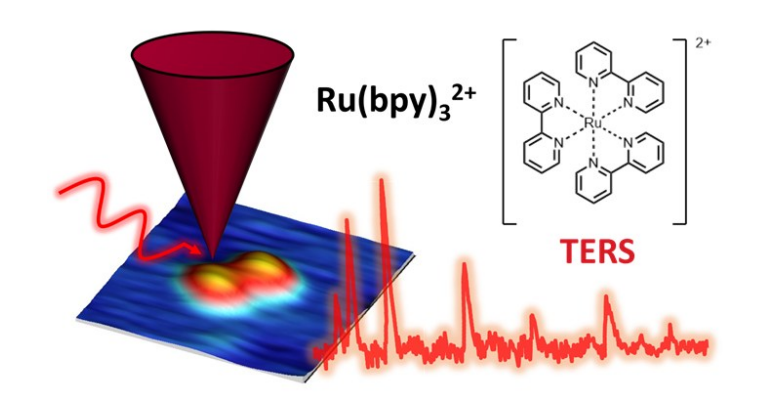


Figure 4. (a) DFT optimized structure (Configuration 1) of Ru(bpy)₃²⁺ molecules on the Cu(100) surface (top view). The dipole moment is calculated to be 0.15 D in the X-direction. (b) Five different types of dipole-dipole interactions according to dipole phase relation. (c) Energy level of five different types of interactions for two molecules. Type 1 is the most energetically favorable.



TOC Graphics